

# Bioinspired Hyaluronic Acid-Based Hydrogel Fuels Bi-Directional Lung Organoid Maturation via PIEZO1 and ITGB1 Mediated Mechanosensation

Junyao Zhang, Daniele Marciano, Lei Wang, Weiwei Wang, Manfred Gossen, Mengting Yang, Tingying Peng, Julien Gautrot,\* Xun Xu,\* and Nan Ma\*

Lung diseases are one of the leading causes of global mortality. Advances in induced pluripotent stem cell (iPSC) differentiation have enabled the creation of bronchiolar and alveolar lung organoids, advancing research on lung conditions. Traditional Matrigel encapsulation, reliant on the spontaneous assembly and propagation of cells with limited external intervention, often results in variability and low reproducibility. The absence of hyaluronic acid (HA) in Matrigel, a key lung extracellular matrix component, limits bronchiolar and alveolar cell differentiation, reducing the efficacy and reproducibility of iPSC-derived organoid generation. To address this, a novel hybrid hydrogel combining HA and 23% Matrigel, inspired by the natural lung environment, is developed. This hydrogel offers improved biochemical support and viscoelastic properties, significantly accelerating organoid development. Within eight days, the hydrogel produces uniformly sized organoids containing both bronchiolar and alveolar epithelial cells. Increased levels of active mechanosensors and transducers, including PIEZO1, Integrin, and Myosin, suggest that the hydrogel's altered viscoelasticity triggers a mechanotransduction cascade. This bioinspired hydrogel provides a robust, fast model for biomedical research, facilitating rapid drug screening, respiratory disease treatment studies, and surfactant trafficking investigations. Furthermore, it enables the exploration of underlying biomechanical mechanisms to enhance the controllability of organoid generation and maturation.

## 1. Introduction

Respiratory system disorders represent a significant and escalating public health concern, constituting a leading cause of death globally.<sup>[1]</sup> These disorders encompass a spectrum of conditions, from congenital anomalies to acquired diseases, influenced by factors like genetics, infections, smoking, and environmental pollutants.<sup>[2]</sup> Despite advancements in biomedical research, effective treatments for numerous lung diseases remain elusive, underscoring the pressing requirement for innovative research models to expand our comprehension of the underlying mechanisms and to devise novel therapeutic approaches.<sup>[3]</sup>


The development of organoids represents a significant technological breakthrough in disease modeling and drug discovery. These miniaturized organs faithfully replicate essential functional and structural features of their in vivo counterparts, offering sophisticated in vitro systems that mirror organ complexity.<sup>[4]</sup> Studies have suggested that induced pluripotent stem cell (iPSC)

J. Zhang, L. Wang, M. Yang, N. Ma  
Institute of Chemistry and Biochemistry  
Free University of Berlin  
14195 Berlin, Germany  
E-mail: [nan.ma@hereon.de](mailto:nan.ma@hereon.de)

J. Zhang, L. Wang, W. Wang, M. Gossen, X. Xu, N. Ma  
Institute of Active Polymers  
Helmholtz-Zentrum Hereon  
14513 Teltow, Germany  
E-mail: [xun.xu@hereon.de](mailto:xun.xu@hereon.de)

D. Marciano, J. Gautrot  
School of Engineering and Materials Science  
Queen Mary University of London  
London E1 4NS, UK  
E-mail: [j.gautrot@qmul.ac.uk](mailto:j.gautrot@qmul.ac.uk)

T. Peng  
Institute for Computational Biology  
Helmholtz Munich  
85764 Neuherberg, Germany

 The ORCID identification number(s) for the author(s) of this article can be found under <https://doi.org/10.1002/admi.202400194>

© 2024 The Author(s). Advanced Materials Interfaces published by Wiley-VCH GmbH. This is an open access article under the terms of the [Creative Commons Attribution](https://creativecommons.org/licenses/by/4.0/) License, which permits use, distribution and reproduction in any medium, provided the original work is properly cited.

DOI: 10.1002/admi.202400194

derived organoids can serve as a valuable tool for investigating lung development, pathogenesis, and exploring effective treatments.<sup>[5]</sup> Currently, the standard lung organoid formation procedure involves definitive endoderm (DE), forming anterior foregut endoderm (AFE) spheroids, and specifying lung progenitors within the spheroids to generate airway bronchial or respiratory alveolar cells.<sup>[6]</sup> However, this method relies heavily on the use of Matrigel, a complex animal-derived extracellular matrices (ECM), which consist, among others, of laminin, type IV collagen, nidogen, and heparan sulfate, growth factors and matrix metalloproteinases. The lack of well-defined composition is the cause of the observed high batch-to-batch variation.<sup>[7]</sup> Moreover, organoid formation depends largely on the intrinsic self-organization of cells with minimal control from external cues. This leads to inefficient and time-consuming organoid development characterized by low reproducibility and shape heterogeneity.<sup>[8]</sup>

To tackle these challenges, the development of a tailored matrix-based support system with specific chemical and biomechanical properties matching the desired organ is crucial. The lung's viscoelastic properties play a fundamental role in regulating cellular behavior during organogenesis *in vivo*.<sup>[9]</sup> Hyaluronic acid (HA), a glycosaminoglycan absent in Matrigel, is a major component of the lung interstitium and alveolar space (Figure 1). It contributes to the maintenance of a viscoelastic cushion, regulates tissue hydration, lubricates biointerfaces, and plays essential roles in tissue homeostasis, cell adhesion, migration, proliferation, immune regulation, and extracellular matrix remodeling.<sup>[10]</sup> Recent advancements in hydrogel research offer promising approach for enhancing and refining organoid generation, as hydrogels can be customized to replicate the chemical composition and viscoelastic properties of the relevant organ's *in vivo* niche.<sup>[11]</sup>

To better replicate the natural lung microenvironment in terms of ECM composition and viscoelasticity, we developed a novel hybrid HA-based hydrogel combining poly(ethylene glycol) dithiol crosslinked HA (HA-PEGDT) with 23% v/v Matrigel. We hypothesized that this hybrid hydrogel would provide a physiologically more relevant matrix for supporting lung organoid generation and maturation. HA hydrogel and Matrigel alone were used as reference materials to discern the unique functions of hybrid HA-based hydrogels. We compared the viscoelastic properties of all hydrogels using photorheology. We monitored the DE differentiation via tracking signature marker expression both at the mRNA and protein level. We evaluated the quality of iPSC-derived AFE spheroids by detecting the existence of FOXA2+NKX2.1+ lung progenitors. The high-quality AFE was then selected and encapsulated in HA-PEGDT, HA-PEGDT-Matrigel, and Matrigel to initiate organoid formation. The impact of HA-PEGDT-Matrigel on lung organoid development was assessed by tracking the morphological changes, visualizing, and quantifying the SOX2+ bronchial cells, CCSP+ airway club cells, CPM+ alveolar epithelial progenitors, and SPC+ mature alveolar epithelial cells in the spheroids. Comparative analysis between HA-PEGDT-Matrigel and Matrigel-derived organoids for mechanosensitive proteins (PIEZO1 and Integrin  $\beta$ 1 (ITGB1)) at the cell-matrix interface and their associated intracellular partners, including RRAS and nonmuscle myosin IIa (NMHC IIA), was conducted to elucidate the underlying mechanisms gov-

erning organoid development. As a result, the bioinspired HA-PEGDT-Matrigel can instruct and accelerate the synergistic maturation of lung organoids toward bi-directional specification of bronchial and alveolar tissues through PIEZO1 and ITGB1-mediated mechanosensing and mechanotransduction. This approach improves controllability and efficiency of lung organoid generation, advancing the prospects of high-throughput drug and vaccine screening, as well as facilitating rapid and in-depth research on the pathogenesis of respiratory disorders.

## 2. Results and Discussion

### 2.1. Enhancement of the Viscoelasticity of Hybrid HA-Based Hydrogel

Utilizing the norbornene-functionalized HA (HA-NB) backbone, the formation of HA-PEGDT hydrogel and HA-PEGDT-Matrigel was achieved by photoinitiated thiol-ene click reactions, facilitating crosslinking to introduce a long-lasting mechanical integrity. To further promote cell adhesion, an RGD peptide (GC-GYGRGDSPG) was incorporated into this system (Figure 1B). To assess the curing and mechanical properties of the resulting hydrogels, we conducted photorheology analysis. Following a short period of equilibration of the system, we monitored the evolution of storage ( $G'$ ) and loss shear moduli ( $G''$ ) during and after UV exposure. Upon UV exposure, the moduli of HA-PEGDT increased rapidly and reached a plateau within 50 s (Figure 1C). The incorporation of 23% v/v Matrigel to HA-PEGDT accelerated the curing process while reduced their storage modulus presumably due to decreased efficiency in the coupling reaction with Matrigel components compared to PEGDT. Nevertheless, the moduli of HA-PEGDT-Matrigel remained higher than solidified Matrigel alone (Figure 1D). Notably, the elasticity of HA-PEGDT-Matrigel is comparable to that of the native human lung ECM ( $\approx 200$  Pa),<sup>[12]</sup> allowing it to generate mechanical forces akin to those in the natural lung tissue environment. This can trigger appropriate mechanosensing and signaling transduction in iPSC-derived lung progenitors. Additionally, the presence of HA in the hydrogel provides proper biochemical cues at the interface between the matrix and cells.

### 2.2. Validation of DE Lineage Commitment

Generation of iPSC-derived lung organoid can be simply separated into two distinct culture conditions,<sup>[5]</sup> the "2D stage", characterized by self-renewal and differentiation of iPSCs on Geltrex-coated substrates, and the subsequent "3D growth stage", where the autonomously formed spheroids containing the lung progenitor cells were encapsulated within either Matrigel and HA-based hydrogels. In brief, iPSCs initially undergo lineage commitment toward the DE, which subsequently differentiates to form the AFE spheroids in the presence of SB43152, Noggin, SAG, FGF2, and CHIR99021. With extended culture period of 3D encapsulation inside the Matrigel and hydrogel with sufficient growth factors, the specification of lung bronchial and alveolar epithelial cells can be accomplished (Figure 2A).

The initial cellular state and stemness of the stem cells play a predominant role in determining the efficacy and success of

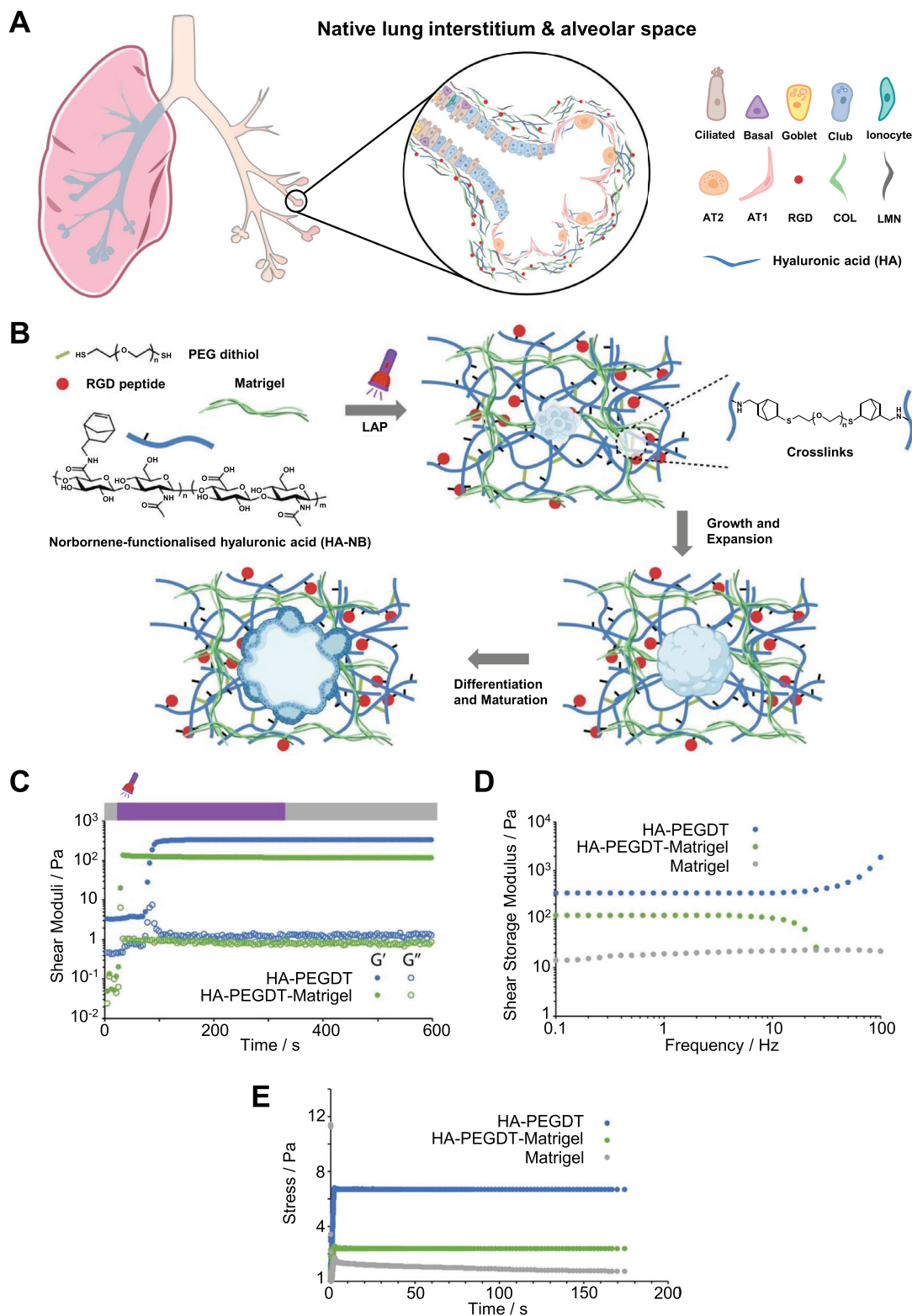


**Figure 1.** Design and characterization of viscoelasticity of HA-based hydrogels. A) Schematic representation of the cell types and extracellular matrix components including HA in native lung. HA is a major ECM component found in both the lung interstitium and alveolar space. B) The hydrogel formation and chemical structure of the HA-NB and PEGDT crosslinker. C) Time sweep profiles of HA-PEGDT with and without Matrigel, from photo rheology experiments (strain, 0.4%; frequency, 1 Hz). D) Frequency sweep profiles of HA-PEGDT, HA-PEGDT-Matrigel, and Matrigel samples (0.4% strain).

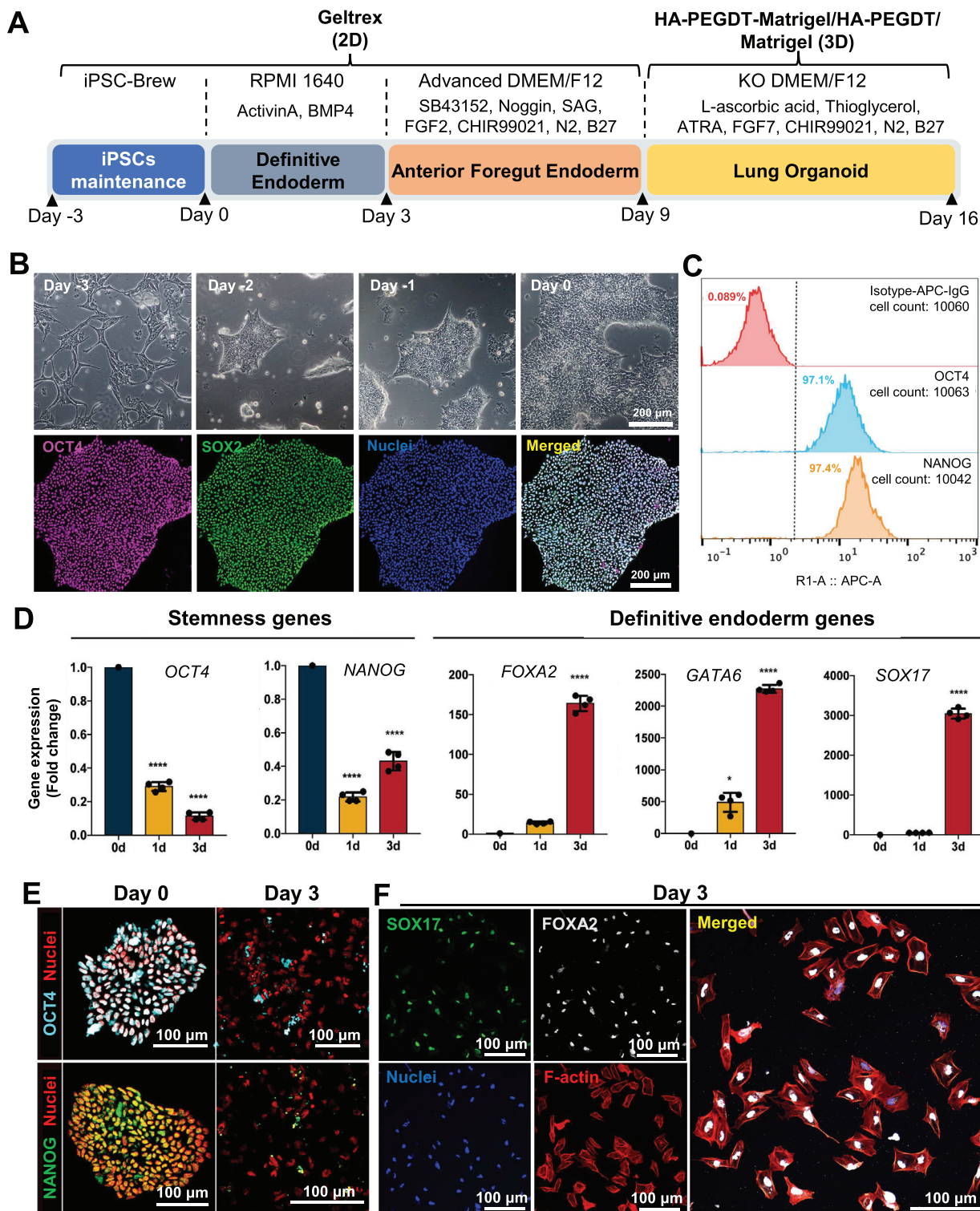


**Figure 2.** Validation of iPSC stemness and DE lineage commitment. A) Schematic summary of bi-directional lung organoid differentiation and maturation process. B) Bright field images showing the morphological changes of iPSCs before induction from day  $-3$  to day 0. Representative immunofluorescence images presenting the preservation of stemness markers (OCT4 in magenta, SOX2 in green, nuclei in blue). Scale bar: 200  $\mu\text{m}$ . C) Quantification of OCT4 and NANOG expression via flow cytometry. D) Quantitative real-time PCR assay for tracking the expression of stemness genes (OCT4 and NANOG) and DE specific genes (FOXA2, GATA6, and SOX17) ( $n = 4$ ,  $*p < 0.05$ ,  $****p < 0.0001$ , One-way ANOVA with Bonferroni's multiple comparisons test). E) Immunostaining for stemness markers including OCT4 (cyan), NANOG (green). Cell nuclei were labeled in red. Scale bar: 100  $\mu\text{m}$ . F) Immunofluorescence-based identification of DE lineage markers containing SOX17 (green) and FOXA2 (white). The nuclei (blue) and F-actin (red) were stained with Hoechst 33342 and CellMask Orange Actin Tracking Stain, respectively. Scale bar: 100  $\mu\text{m}$ .

subsequent organoid formation. Here, iPSCs were seeded on Geltrex-coated culture plates three days before induction (day –3). The typical morphology of iPSC colonies, characterized by condensed cell population and distinct edges of cell clusters was observed. When the cell confluency reached 80–90%, immediately before induction (day 0), the majority of iPSCs retained their stemness as demonstrated by immunostaining of OCT4+ SOX2+ cells (Figure 2B), with over 97% of iPSCs being OCT4+ and NANOG+ according to flow cytometry (Figure 2C). To monitor DE differentiation, cells were collected at the indicated time points and further lysed or fixed for quantitative analysis of stemness and endoderm markers. As induction progressed, the expression of stemness markers including OCT4 and NANOG were remarkably decreased, although there was fluctuation in NANOG mRNA expression was exhibited at day 3, the protein level of NANOG was significantly decreased (Figure 2D,E). Contrarily, the levels of DE-specific markers increased, both at mRNA and protein levels (Figure 2D,F).

### 2.3. Creation of High-Quality Foregut Spheroids

Nkx2.1 has been identified as a marker for progenitors of both thyroid and lung, whereas Foxa2 serves as a stringent marker for cells capable of generating lung epithelial cells, as evidenced by previous *in vivo* studies.<sup>[13]</sup> In our work, the presence of FOXA2+ NKX2.1+ lung progenitors in the majority region of AFE indicated the formation of high-quality spheroids (Figure 3A,B).

To minimize the influence of initial spheroid morphological variation on organoid formation, on day 9 after DE induction, AFE spheroids from the same batch with similar size and shape were selected and embedded in Matrigel, HA-PEGDT hydrogel, and HA-PEGDT-Matrigel respectively. By day 16, eight days following encapsulation, several AFE spheroids from the Matrigel group demonstrated a notable increase in size and exhibited folded structures. Those embedded in HA-PEGDT-Matrigel progressed to form spherical cysts consisting of a thin layer of cuboidal cells. However, AFE spheroids embedded in HA-PEGDT failed to develop advanced structures and experienced a decline in viability (Figure 3C). This observation implies that the shear moduli of HA-PEGDT may not be conducive to supporting lung organoid formation. The incorporation of Matrigel seems to relieve the mechanical constraints of HA-PEGDT while maintaining an appropriate viscoelasticity intermediate between pure Matrigel and HA-PEGDT as illustrated in Figure 1C,D. Cell death and dispersion of individual cells within spheroids embedded in the HA-PEGDT hydrogel, individual cells scattered, preventing spheroid were apparent, as observed through bright field imaging revealing bright refraction spots with distinct boundaries (Figure 3C). This phenomenon obstructed the harvesting and subsequent cultivation of spheroids. Subsequent experiments only focused on the HA-PEGDT-Matrigel and Matrigel groups.

Further, image-based quantification of spheroid size parameters, including major axis, minor axis, and aspect ratio, revealed that immediately post encapsulation and after eight days of culture in hydrogels or Matrigel, the length of the major axis of spheroids was significantly decreased in the HA-PEGDT-Matrigel group. The formation of more homogeneous and compacted organoids in HA-PEGDT-Matrigel compared to those in

Matrigel was supported by the decreased standard deviation. The aspect ratio approaching values close to 1 in organoids from HA-PEGDT-Matrigel indicated enhanced circularity (Figure 3D,E).

Although the spheroid morphology and size became uniform, starting from day 16, the spheroid diameter was limited to 200  $\mu\text{m}$ . Due to the mechanical properties of HA-PEGDT-Matrigel, the spheroids could not continue to grow over time, leading to high cell density, which might cause cell apoptosis. This can hinder the later branching of organoids and pose a series of challenges for broader applications. To address these limitations, our future research will focus on developing slowly degradable crosslinkers for HA-PEGDT-Matrigel. These crosslinkers should gradually degrade as the spheroids increase in size, providing a more relaxed environment within the hydrogel that allows for proper mechanical stimulation and supports the growth of spheroids and organoids. Additionally, incorporating regularly connected pores within the hydrogel with degradable crosslinkers can help form larger, uniformly sized organoids and prevent organoid merging.

### 2.4. HA-PEGDT-Matrigel Promotes Bi-Directional Lung Organoid Maturation

To further delineate the lung organoids, spheroids from different hydrogels were harvested and cryosectioned for immunofluorescence analysis. The staining results revealed that spheroids in the Matrigel group exhibited weak cytoplasmic distribution of transcription factor SOX2, with none of it translocating into the cell nuclei. Within only 8 days of organoid development,  $\approx 56 \pm 10\%$  of cells in the spheroids from the HA-PEGDT-Matrigel group were identified as SOX2+ proximal conductive airway cells, confirmed by their cell nuclear colocalization (Figure 4A,B). Most of these organoids mainly maintained their spherical morphology with a well-oriented epithelial outer layer, as sustained SOX2 expression has been reported to promote epithelialization while inhibiting lung branching patterns.<sup>[14]</sup> Carboxypeptidase M (CPM), a glycoprotein, serves as a marker for alveolar epithelial progenitors,<sup>[15]</sup> was found at the peripheral region of organoids developed in HA-PEGDT-Matrigel (Figure 4A). Notably, SPC, a marker for specifically defining mature alveolar type 2 (AT2) cells,<sup>[16]</sup> was highly expressed in organoids from HA-PEGDT-Matrigel (Figure 4B). Co-staining of SOX2/CCSP with SPC, or CCSP with CPM in the same spheroid confirmed that simultaneous bi-directional differentiation to both airway bronchial and alveolar epithelium occurred in HA-PEGDT-Matrigel group (Figure 4C). It provides a robust biomedical analysis model that allows for synergistic testing of responses from different parts of the lung within the same system, as well as interactions between cells from different regions. This bi-directionally differentiated lung organoid model can accelerate the testing process and reduce system errors.

Lung development can be classified into five stages, based on our understanding of the *in vivo* processes. Beginning with the embryonic stage, lung buds emerge, followed by the pseudoglandular stage characterized by airway branching and epithelial cell differentiation. The canalicular stage is distinguished by the formation of type I and type II lung epithelial cells. Subsequently, in the saccular stage, lung alveoli are generated.

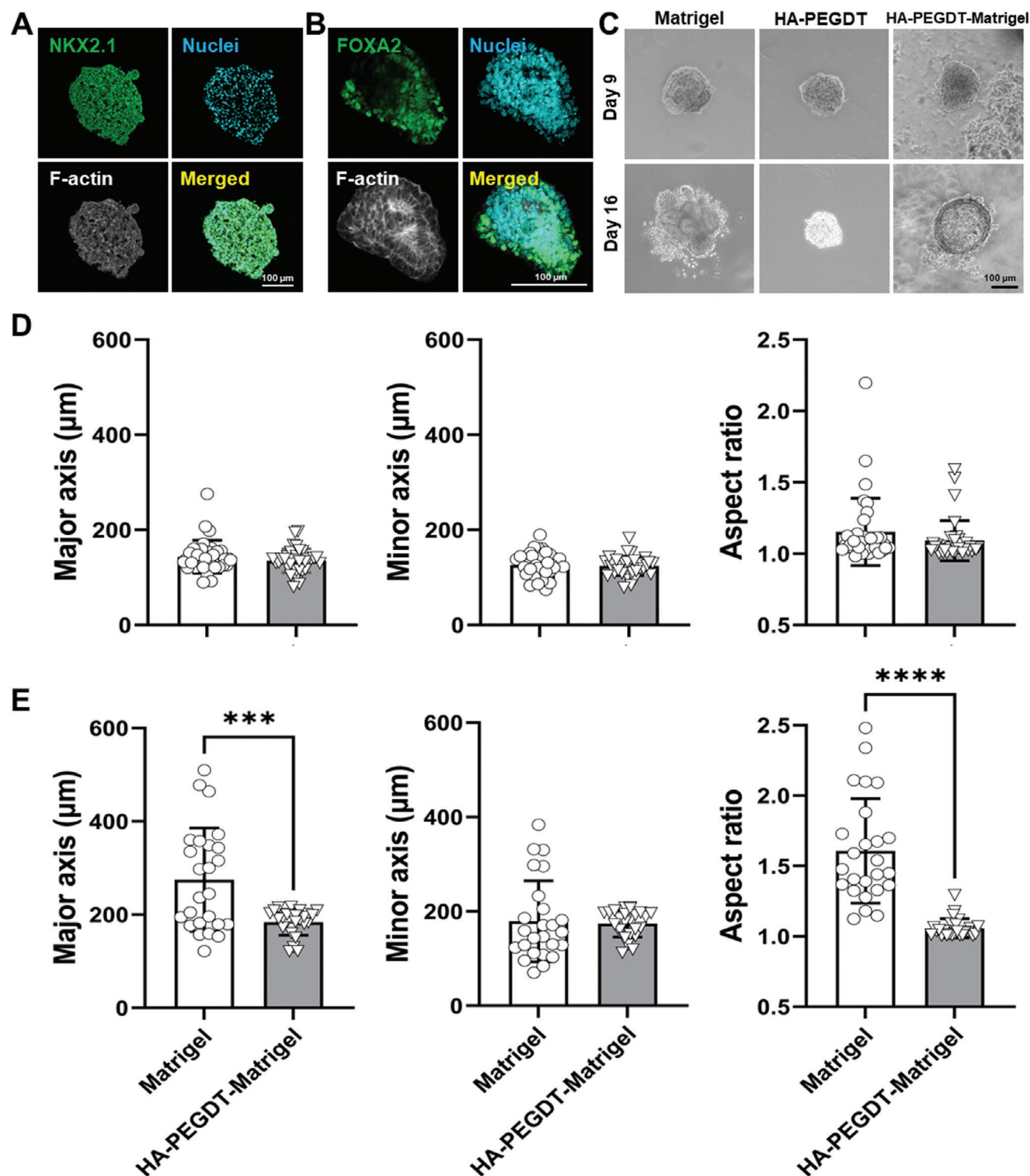


**Figure 3.** Characterization of foregut spheroids before and after embedding in Matrigel and HA-based hydrogel. Representative immunofluorescence of primordial progenitor stage markers A) NKX2.1 (green) and B) FOXA2 (green). C) Representative bright field images showing the corresponding morphological change of the same individual AFE spheroid from day 9 (the day of encapsulation) to day 16 (8 days after encapsulation). The nuclei (cyan) and F-actin (white) were stained with Hoechst 33 342 and CellMask Orange Actin Tracking Stain, respectively. Scale bar: 100  $\mu\text{m}$ . Quantification of the size parameters of spheroids D) on day 9 ( $n = 34$ ) and E) on day 16 ( $n = 25$ ); \*\*\* $p < 0.001$ , \*\*\*\* $p < 0.0001$ , two-tailed unpaired Student t-test.

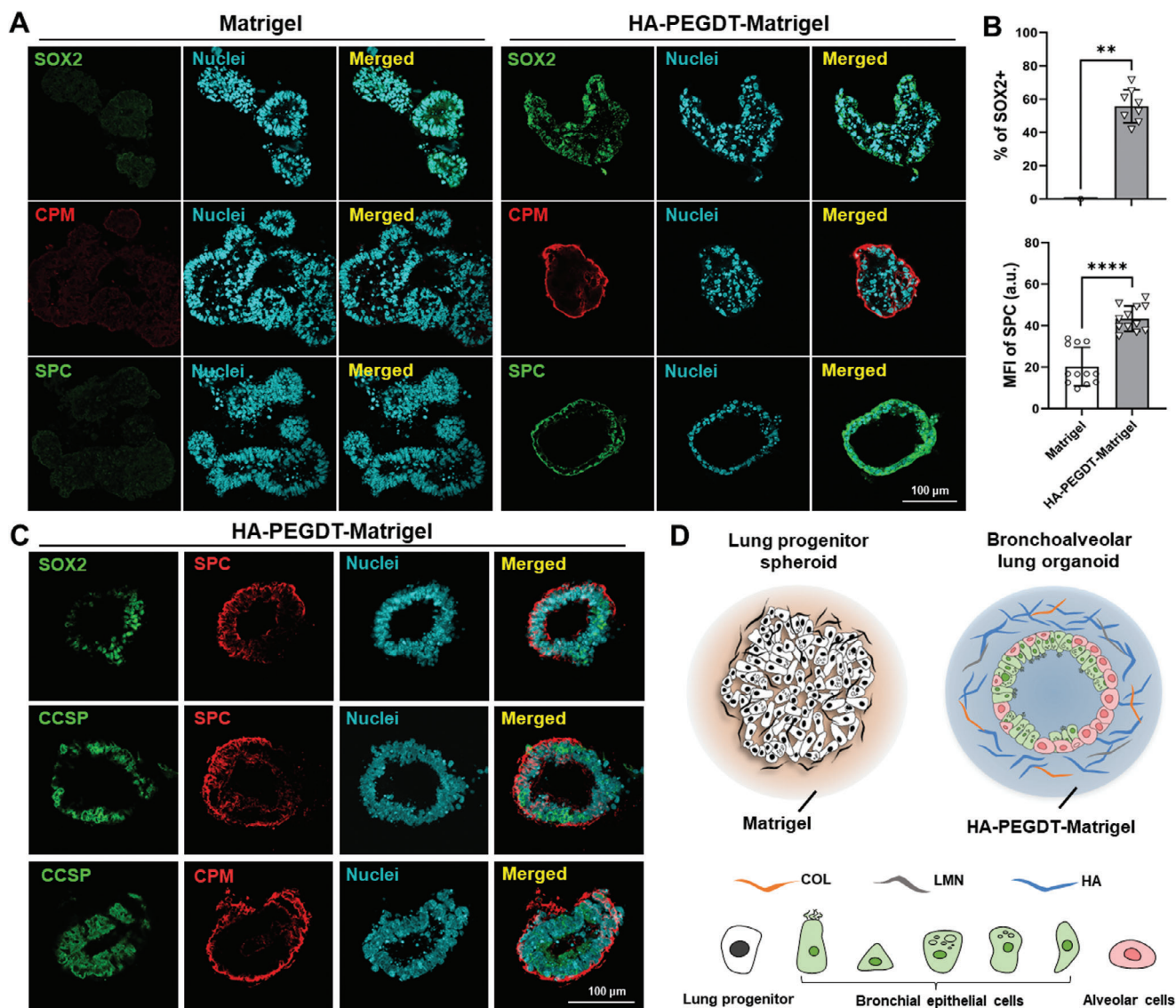


**Figure 4.** Bi-directional lung organoid development in HA-PEGDT-Matrigel. **A)** Representative images showing the expression of SOX2 (green), CPM (red) and SPC (green) in AFE encapsulated in the HA-PEGDT-Matrigel for 8 days (day 16 in total post induction) compared to those in the Matrigel group. The nuclei (cyan) were stained with Hoechst 33 342. Scale bar: 100  $\mu$ m. **B)** Quantitative analysis of SOX2+ proportion and mean fluorescence intensity of SPC in spheroids after 8-days encapsulation (day 16 in total post induction) from indicated groups ( $n = 8$  for SOX2,  $n = 12$  for SPC;  $**p < 0.01$ ,  $****p < 0.0001$ , two-tailed unpaired Student t-test). **C)** Representative co-staining images of airway bronchial markers SOX2, CCSP, and alveolar markers SPC and CPM in AFE encapsulated in the HA-PEGDT-Matrigel for 8 days (day 16 in total post induction). The nuclei (cyan) were stained with Hoechst 33 342. Scale bar: 100  $\mu$ m. **D)** Schematic illustration of the ECM components presented by Matrigel and HA-PEGDT-Matrigel, and proposed cell composition of bi-directionally differentiated lung organoid generated from HA-PEGDT-Matrigel in comparison to the unspecified lung progenitor spheroid derived from Matrigel after 8-day encapsulation (day 16 in total post induction).

Finally, the alveolar stage after birth sees lung ventilation initiation and alveoli expansion.<sup>[17]</sup> Based on observed morphological changes in spheroids and expression patterns of lung-related markers, we propose that spheroids in the HA-PEGDT-Matrigel group have minimally progressed to the transition phase between pseudoglandular and canalicular stages within 8 days post hydrogel encapsulation (equiv. to 16 days from initial iPSC induction), which exhibit bi-directional differentiation, encompassing both proximal airway and distal alveolar structures. Conversely, AFE spheroids with FOXA2 progenitors from the Matrigel group stay

predominantly at the initiation of embryonic stage (Figure 4D). Notably, a minimum of 16 weeks after gestation is required to reach the pseudoglandular/canalicular stage in vivo, whereas in our in vitro bioinspired hybrid HA-based hydrogel system, this stage was achieved with 8 days post hydrogel encapsulation, within 16 days starting from initial iPSC induction in total. This result highlights the possibility of utilizing HA-PEGDT-Matrigel as a matrix to boost the maturation of individual lung organoids containing both bronchial and alveolar cell types in a week time-frame in vitro.

Similar to other studies, our system modified based on the protocol reported from Miller et al.,<sup>[5]</sup> still uses Matrigel or other animal-derived reagents, such as FBS, which remains a barrier for biomedical translation. For DE induction, the commercially available FBS serum-free medium (STEMdiff Definitive Endoderm Medium, STEMCELL Technologies) can be applied in our future study. For organoid formation, despite Dye's establishment of lung organoids in a Matrigel-free system using alginate, maintaining them in alginate hydrogel for more than 5 days resulted in a low health rate of 35%, requiring the addition of Matrigel to restore their state.<sup>[18]</sup> Therefore, finding an alternative to HA-PEGDT-Matrigel or Matrigel remains a challenge that needs to be addressed.

## 2.5. HA-PEGDT-Matrigel Accelerates Lung Organoid Maturation via PIEZO1 and ITGB1 Mediated Mechanosensation

Lung epithelial cells reside at the interface between ECM and the parenchyma. The ECM network, aside from binding and presenting growth factors, offers not only resistance to deformation, but also force transition over distances. During development, epithelial cells in the lung are constantly exposed to various mechanical forces. Alterations in mechanical stresses can profoundly impact lung morphogenesis and regulate alveolar specification.<sup>[19]</sup> As a key mechanosensor, PIEZO1 mediates physiological and pathophysiological changes in the respiratory system and plays a critical role in epithelial homeostasis and lung development.<sup>[20]</sup> Given the high viscoelasticity of HA-PEGDT-Matrigel (Figure 1C), we compared the levels of PIEZO1 and its associated membrane and intracellular proteins in spheroids or organoids derived using the different hydrogel matrices employed in this study. After 8 days of matrix encapsulation. We observed a significant enhancement of PIEZO1, cytoplasmic RRAS, and active conformation of ITGB1 in organoids from HA-PEGDT-Matrigel, indicating PIEZO1-initiated integrin activation via RRAS mediated inside-out signaling (Figure 5A,B). Mechanical stimuli from outside the cell to inside enhanced the level of molecular motor myosin, strengthening the assembly of mechanosensitive integrin-mediated focal adhesion anchorage and evoking PIEZO1 activation to establish a feedforward loop. This could result in the highest increase in NMHC IIA levels among all tested membrane and intracellular molecules (Figure 5B).

Mechanical forces and local biochemical factors synergistically control airway and alveolar epithelial cell morphogenesis and specification.<sup>[21]</sup> We anticipate that PIEZO1 and ITGB1 sense the altered biochemical properties and enhanced shear moduli in HA-PEGDT-Matrigel at the cell-matrix interface, activating NMHC IIA. Intracellularly, RRAS transduces mechanical signals from PIEZO1 to activate ITGB1, regulating NMHC IIA-mediated contractile force.<sup>[22]</sup> Phosphorylation of Myosin II can also increase PIEZO1 activity,<sup>[23]</sup> forming a positive feedback loop involving PIEZO1, Integrin, and Myosin. Meanwhile, both intracellularly and intercellularly, the balance between the WNT-FGF network and the NOTCH pathway is crucial for determining the di-directional differentiation.<sup>[24]</sup> PIEZO1 activates both WNT and FGF pathways, while Myosin inhibits WNT activity.<sup>[25]</sup> Conversely, FGF can activate Myosin and regu-

late ITGB1 degradation.<sup>[26]</sup> Upregulated NOTCH signaling hinders alveolar epithelial cell differentiation.<sup>[27]</sup> Integrin upregulates NOTCH-related molecules, and PIEZO1 activates ITGB1 through RRAS, mediated by the NOTCH pathway.<sup>[22a]</sup> Myosin activity and its mediated contraction are linked to force-dependent NOTCH activation.<sup>[28]</sup> In non-epithelial cells, PIEZO1 can activate NOTCH via ADAM10 and inhibit it via DTX.<sup>[29]</sup> The role of PIEZO1 in NOTCH signaling in our system remains to be explored through in situ spatiotemporal analyses. Although we uniformly added WNT activator and FGF throughout the culture medium, cells in different regions may respond differently to these factors and their gradients, leading to varying levels of NOTCH activation among neighboring cells. This variability may result in the presence of both differentiation directions within a single organoid. This is evident from our results, as SPC+ or CPM+ cells were in the peripheral region, opposite to SOX2+ or CCSP+ cells in organoids (Figure 4C). Therefore, we speculate that the spatiotemporal interactions between the PIEZO1, Integrin, and Myosin loop, along with the WNT, FGF, and NOTCH pathways, accelerate organoid development by specifying NKX2.1+ FOXA2+ lung progenitors into SOX2+, CCSP+ bronchial, CPM+ alveolar progenitor, and mature SPC+ type 2 alveolar lineages in AFE spheroids (Figure 5C). In future work, we will employ single-cell measurements, spatial biological analysis, AI-assisted label-free live-cell tracking, and correlative analysis of multi-modal cell and hydrogel images to gain deeper insights into the molecular mechanisms underlying bi-directional maturation during lung organoid formation. By fine-tuning hydrogel parameters and relevant pathways, we aim to further promote organoid maturation in a more controllable manner.

A few similar HA-based hydrogels have been reported in regenerative medicine studies. The HA hydrogels developed by Loebel et al.,<sup>[30]</sup> although similar to ours, differ in composition, source material, crosslinker, and viscoelasticity. Their hydrogels, modified with laminin/entactin, supported the formation and growth of alveolospheres from 66-day Matrigel derived SPC+ AT2 cells but exhibited similar heterogeneity to Matrigel with less than 40% of cells maintaining SPC+. In our study, HA hydrogels mimic natural lung ECM components and viscoelasticity to rapidly achieve bi-directional differentiation of stem cells into uniformly sized organoids with both bronchial and alveolar cell types. Our approach aims to overcome Matrigel's limitations, including low efficiency, long duration, and high heterogeneity. Notably, from Loebel's study, the 20 kPa engineered microwell HA hydrogels were further created for 2.5D culture to achieve uniformly sized spheres. The AT2 cell proliferative capacity in the spheres was validated in vitro and in injured murine lungs. Their in-depth structured design and validation of function both in vitro and in animal models are valuable for us to learn and apply in our future work, to make the growth, maturation, size, and morphology of our organoids more controllable and functionally defined. HA-based hydrogels have also been applied in the 3D culture of neural progenitor cells (NPCs).<sup>[31]</sup> Although the experimental design and target objectives differ, our research strategies are both derived from the presence of abundant HA in the natural microenvironment of the target cells and the appropriate mechanical properties. Additionally, inspired by their study, we can incorporate the comparison of different mechanical properties of HA hydrogels on cell differentiation and the dynamic



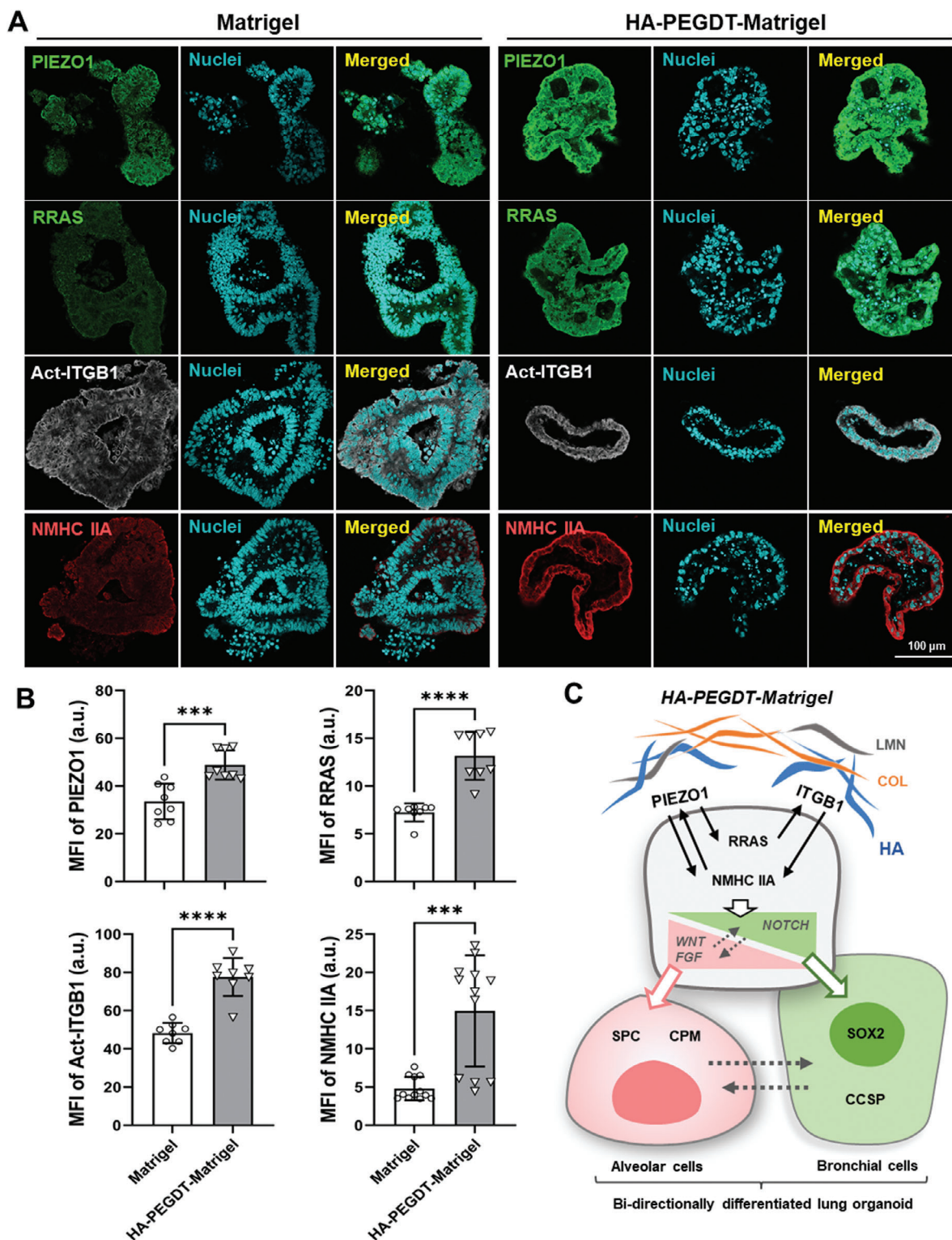


**Figure 5.** Mechanosensation of lung organoids growing in HA-PEGDT-Matrigel. A) Representative images showing the expression of PIZEO1 (green), RRAS (green), Act-ITGB1 (white) and NMHC IIA (red) in AFE encapsulated in the HA-PEGDT-Matrigel for 8 days (day 16 in total post induction) compared to those in the Matrigel group. The nuclei (cyan) were stained with Hoechst 33 342. Scale bar: 100  $\mu$ m. B) Quantification of the mean fluorescence intensity alteration in PIZEO1, RRAS, Active ITGB1 and NMHC IIA levels in spheroid from indicated groups after 8-day encapsulation (day 16 in total post induction) ( $n = 8$  for PIEZO1, Act-ITGB1 and RRAS;  $n = 12$  for NMHC IIA; \*\*\* $p < 0.001$ , \*\*\*\* $p < 0.0001$ , two-tailed unpaired Student t-test). C) Scheme of the proposed underlying mechanism of HA-PEGDT-Matrigel derived lung organoid from spheroid-hydrogel interface to the intracellular events in response to biomechanical stimulation.

tracking of hydrogel degradation into our future mechanistic analysis.

Our HA-PEGDT-Matrigel accelerates lung organoid maturation, potentially shortening drug screening and vaccine development times. The presence of both airway and alveolar cell types in the same organoid allows for efficient analysis of infectious diseases and fibrosis. However, these organoids still lack the cellular composition and functionality of mature adult lungs. The ECM's biochemical, geometrical, and mechanical properties are crucial for cell differentiation, varying across organs, regions of organs, and pathophysiological conditions. This highlights the need for engineered hydrogels to promote lung organoid maturation. Future work will create microstructures, adjust crosslinker concentrations and the HA-to-Matrigel ratio, and explore collagen- and laminin-based biomaterials as replacements for Matrigel to better mimic authentic pathological and physiological conditions.

### 3. Conclusion

To ensure rapid, effective, and stable generation of iPSC-derived lung organoids, and to address issues of heterogeneity and low reproducibility associated with conventional Matrigel encapsulation methods, a novel hybrid HA-based hydrogel was developed by recapitulating natural lung ECM composition. Utilizing click chemistry, we successfully synthesized the HA hydrogel and hybrid hydrogel combining HA and 23% v/v Matrigel, termed as HA-PEGDT and HA-PEGDT-Matrigel, respectively. In addition, the shear modulus of both HA-PEGDT and HA-PEGDT-Matrigel was also enhanced compared to Matrigel. The high-quality human iPSC-derived foregut spheroids presenting FOXA2+ NKX2.1+ lung progenitors from the same batch, were served as the source spheroids for further encapsulation with HA-PEGDT, HA-PEGDT-Matrigel, and Matrigel. HA-PEGDT-Matrigel promoted bi-directional lung organoid development within 8 days post hydrogel encapsulation, as evidenced by the formation of spherical cysts consisting of SOX2+ proximal conductive airway cells, CPM+ alveolar epithelial progenitors and SPC+ mature alveolar epithelial cells. Further mechanistic analysis in organoids derived from HA-PEGDT-Matrigel, compared to those from Matrigel, revealed significant enhancement of PIEZO1, RRAS, NMHC IIA protein level and high activity of ITGB1, indicating the potential effects of mechanosensitive integrin activation and myosin-mediated contractile force generation on accelerating specification process of lung progenitors into conductive airway epithelial cells and mature alveolar lineages in iPSC-derived organoids. Overall, we demonstrated the substantial impact of HA-PEGDT-Matrigel on the formation and maturation of iPSC-derived lung organoids. Notably, the hybrid hydrogel combining HA and Matrigel with optimal shear moduli, rather than the HA hydrogel with high moduli or the Matrigel with low moduli, can effectively promote organoid formation. This emphasizes the predominant role of biomechanics and biochemical properties of the matrix in organoid fate determination and unveils the mechanisms behind controllable organoid formation. Although the deeper underlying mechanism, such as the crosstalk of WNT and NOTCH signaling with mechanosensing and transduction pathways, should be further explored, these results highlight the hybrid HA-based hydrogel. Designed by drawing inspi-

ration from nature but functionalized to go beyond natural processes, this hydrogel accelerates organoid maturation toward both bronchial and alveolar lineages within a week. This offers promising implications for large-scale high-throughput drug screening, vaccine development, and lung disease modeling.

### 4. Experimental Section

**Synthesis of Norbornene-Functionalized HA (HA-NB):** Sodium hyaluronate (0.2 g,  $5.27 \times 10^{-1}$  mmol based on repeating units; Mw:  $2 \times 10^5$  g mol<sup>-1</sup>; Sigma-Aldrich, Germany) was dissolved in 20 mL of MES buffer (0.1 M, pH 5.5). The solution was purged with nitrogen and then EDC-HCl (0.148 g,  $7.72 \times 10^{-1}$  mmol) and NHS (0.089 g,  $7.72 \times 10^{-1}$  mmol) were added in one portion and left to stir for 10 min. Subsequently, the pH of the solution was increased to  $\approx 8.0$  using NaOH (300 mL of a 2 M stock). 5-norbornene-2-methylamine (0.1 mL,  $8.12 \times 10^{-1}$  mmol) was injected into the reaction mixture, using a syringe, while stirring under nitrogen atmosphere. The resulting mixture was left to stir overnight at room temperature. NaCl (0.75 g, 12.8 mmol) was then added to the reaction solution to neutralize the reaction product and form sodium hyaluronate derivatives. The reaction solution was then precipitated into tenfold excess cold acetone (4 °C). The precipitate was filtered and then redissolved in 20 mL of deionized water and dialyzed against deionized water by changing the dialyzate every 24 h for 5 days. Finally, the solution was frozen at  $-80$  °C and lyophilized to yield HA-NB. The degree of functionalization of HA-NB was determined via <sup>1</sup>H NMR spectroscopy (14.5%). <sup>1</sup>H NMR (D<sub>2</sub>O):  $\delta$ , 6.33 and 6.02 ppm (norbornene vinyl protons, endo), 6.26 and 6.23 ppm (norbornene vinyl protons, exo), 1.9 ppm (actyl protons).

**HA-PEGDT Hydrogel Formation:** HA-PEGDT hydrogels were formed via a thiol-ene reaction initiated by near ultraviolet (UV) light exposure using poly(ethylene glycol) dithiol (PEGDT, Sigma-Aldrich, Germany) as crosslinker. HA-NB was dissolved in PBS (1.25% w/v) and PEGDT was added to achieve a ratio of thiol: norbornene of 1:2.66 (crosslinking density: 37.5%). The resulting solutions were then irradiated under UV light in the presence of the radical photoinitiator lithium phenyl-2,4,6-trimethylbenzoylphosphine (LAP, Sigma-Aldrich, Germany) at 10% of the total crosslinker molarity (i.e., mmol LAP: mmol PEGDT = 1:10). A thiolated cell-adhesive RGD peptide (GCGGRGDSFG, ProteoGenix, France) was added at a concentration of 1.07 mM. The UV light exposure was at 17 mW cm<sup>-2</sup> for 120 s, using an Omnicure series 2000 lamp ( $\lambda$ : 320 to 500 nm, calibrated with an ILT 1400-A radiometer).

**HA-PEGDT-Matrigel Formation:** Matrigel (original protein concentration: 8.8 mg mL<sup>-1</sup>; Corning Inc., USA; Cat. Number 356 234, Lot Number 024 6001) was diluted with PBS to a protein concentration at 4 mg mL<sup>-1</sup> as a working solution. Incorporate an appropriate volume of the Matrigel working solution into HA-PEGDT solution ingredients to achieve a final protein concentration of 2 mg mL<sup>-1</sup> (equiv. to 23% v/v of original Matrigel), while maintaining other components and conditions unchanged. After UV irradiation at 17 mW cm<sup>-2</sup> for 120 s, using an Omnicure series 2000 lamp ( $\lambda$ : 320 to 500 nm, calibrated with an ILT 1400-A radiometer). The hybrid HA-PEGDT-Matrigel was formed.

**Photorheology:** Rheological measurements were performed using a hybrid rheometer (DHR-3) from TA Instruments fitted with a UV accessory. 100  $\mu$ L solutions of hydrogel precursors were placed between an upper parallel standard Peltier plate geometry (20 mm) and a bottom quartz window (allowing transmittance of UV light) at a fixed gap of 250  $\mu$ m. UV irradiation (Omnicure S1500 mercury lamp,  $\lambda$ : 280–600 nm, connected via a light guide and calibrated with an ILT 1400-A radiometer) was started after a period of oscillation (30 s) to equilibrate the system. To identify the gelation point and monitor the crosslinking progression, time sweep measurements (10 min) at a controlled strain of 0.4% and a constant angular frequency of 1 Hz (6.28 rad s<sup>-1</sup>) were performed, at room temperature. Storage ( $G'$ ) and loss moduli ( $G''$ ) were recorded as a function of time using the TRIOS software. Subsequently, a frequency sweep was carried out, recording  $G'$  and  $G''$  as a function of frequency in a range of 0.1–100 Hz at

0.4% strain. Amplitude sweeps were carried out at an oscillating frequency of 1 Hz. Finally, stress relaxation measurements were carried out and gels were subjected to 2.0% strain, which was reached in 2 s, and held for 180 s.

**Rheology of Matrigel:** Rheological measurements were performed using a hybrid rheometer (DHR-3) from TA Instruments. Matrigel was thawed overnight on ice in a refrigerator. All measurements were carried out using a parallel-plate configuration, samples were placed on a fixed plate pre-heated at 37 °C for 15 min to ensure gelation. Then, a frequency sweep was carried out, recording the storage ( $G'$ ) and loss moduli ( $G''$ ) as a function of frequency in a range of 0.1–100 Hz at 10% strain.

**Cell Line:** Human iPSC cell line BIHi001-A (RRID: CVCL\_IT54) was a treasured gift from Dr. Harald Stachelscheid, Stem Cell Core Facility, Berlin Institute of Health at Charité, Berlin, Germany. Detailed information on this cell line can be found in hPSCreg database, which is accessible at <http://hpscereg.eu/cell-line/BIHi001-A>.

**iPSC Maintenance:** Culture conditions of human iPSC were previously described.<sup>[32]</sup> Briefly, one well of a 6-well plate was coated with 1 mL Geltrex (A14133-01, Thermo Fisher Scientific, Germany) at a final protein concentration of 225  $\mu\text{g mL}^{-1}$  at 37 °C for 1 h before cell seeding. All iPSCs were incubated at 37 °C in a humidified atmosphere containing 5% v/v CO<sub>2</sub>. StemMACS iPS-Brew XF medium (130-101-375, Miltenyi Biotec, Germany) was used as a basic medium to maintain the stemness of iPSC and was changed daily. On the first day of seeding, ROCK inhibitor Y-27632 (10  $\mu\text{M}$ ; 146986-50-7, MedChemExpress LLC, USA) was added to the basic medium to facilitate the cell recovery, and it was subsequently removed in the following days. When the confluency reached 70–80% (3–4 days) in a well, the cells should be passaged.

**iPSC Passaging:** ReLeSR (100-0484, STEMCELL Technologies GmbH, Germany) was used according to the manufacturer's instructions. Briefly, 1 mL per well of ReLeSR solution was applied and aspirated within 1 min. The plate was incubated at 37 °C for 2 min and the colonies were detached by adding and rinsing with 1 mL of iPS-Brew XF medium per well. Then, the colonies were transferred to a 15 mL conical tube containing iPS-Brew XF medium supplemented with 10  $\mu\text{M}$  Y-27632. Finally, the suspended cell aggregates were split at a ratio of 1:6 to individual wells of a 6-well plate.

**DE Induction:** The protocol of DE induction was described previously.<sup>[33]</sup> In short, BMP4 (130-111-168, Miltenyi Biotec, Germany) and Activin A (130-115-013, Miltenyi Biotec, Germany) comprise the primary elements of the inducing medium, while fetal bovine serum (FBS, FBS.S.0615; Bio&SELL GmbH, Germany) was employed to moderate apoptosis and enhance induction efficacy. On day 1, cells were treated with 50 ng mL<sup>-1</sup> BMP4 and 100 ng mL<sup>-1</sup> Activin A in RPMI 1640 media (11 875 093, Thermo Fisher Scientific, Germany) without FBS. The cells were then treated with freshly prepared 100 ng mL<sup>-1</sup> Activin A in RPMI 1640 media for the next two days, with increasing concentrations of 0.2% and 2% FBS.

**AFE Spheroid Formation and Hydrogel Embedding:** After DE lineage commitment, AFE spheroids were generated as previously described, with slight modifications.<sup>[5]</sup> Briefly, SB431542 (10  $\mu\text{M}$ ; 130-106-543, Miltenyi Biotec, Germany), FGF2 (500 ng mL<sup>-1</sup>; 130-093-564, Miltenyi Biotec, Germany), Noggin (200 ng mL<sup>-1</sup>; 130-103-455, Miltenyi Biotec, Germany), SAG (1  $\mu\text{M}$ ; T4211, Target Molecule Corp, Germany) and CHIR99021 (2  $\mu\text{M}$ ; 130-103-926, Miltenyi Biotec, Germany) were added into Advanced DMEM/F12 medium (12 634 010, Thermo Fisher Scientific, Germany) supplied with N-2 (1x; 17 502 048, Thermo Fisher Scientific, Germany), B27 (1x; 17 502 048, Thermo Fisher Scientific, Germany), HEPES (10  $\mu\text{M}$ ; 15 630 056, Thermo Fisher Scientific, Germany), GlutaMAX (1x; 35 050 061, Thermo Fisher Scientific, Germany) and Penicillin-Streptomycin (1x; 15 140 122, Thermo Fisher Scientific, Germany) to form a complete AFE inducing medium. DE was treated with AFE induction medium for 6 days. The supernatant containing floating AFE spheroids, generated from iPSC-derived DE, was collected into a 15 mL conical tube and then sequentially filtered through 200 and 100  $\mu\text{m}$  filters (pluriSelect Life Science, Germany) to select uniform AFE spheroids  $\approx$  100–200  $\mu\text{m}$  in size. The spheroids were then mixed with different hydrogel solutions at a concentration of 5 spheroids  $\mu\text{L}^{-1}$ . Next, 20  $\mu\text{L}$  of the hydrogel solution

was dropped onto a culture dish and solidified by either heating (for Matrigel) or UV irradiation (for HA-based hydrogels).

**Bi-Directional Lung Organoid Development:** The inducing of lung organoids was carried out as previously described.<sup>[5]</sup> Briefly, the embedded AFE spheroids were exposed to the induction medium consisting of KnockOut DMEM/F-12 (12 660 012, Thermo Fisher Scientific, Germany) as basal medium supplemented with N2, B27, GlutaMAX, Penicillin-Streptomycin, Bovine serum albumin (BSA; A2153, Sigma-Aldrich, Germany), Ascorbic acid (50 ng mL<sup>-1</sup>; A4544, Sigma-Aldrich, Germany), 1-Thioglycerol (0.4  $\mu\text{M}$ ; 202-495-0, Sigma-Aldrich, Germany), FGF7 (10 ng mL<sup>-1</sup>; 130-093-849, Miltenyi Biotec, Germany), Retinoic Acid (50 nM; 130-117-339, Miltenyi Biotec, Germany) and CHIR-99021 (3  $\mu\text{M}$ ; 130-103-926, Miltenyi Biotec, Germany) to generate a bi-directionally differentiated lung organoid. The medium was changed every other day.

**Quantitative Analysis of Spheroid Size and Morphology:** To compare the morphological differences and uniformity of spheroids formed in different hydrogels at various time points, bright-field microscopy imaging at 200x magnification was performed on spheroids from three hydrogel domes of each group, representing independent biological experiments, on days 9 and 16. The original-sized Tif images were imported into ImageJ software (NIH, USA). The major axis (the longest line segment passing through the spheroid) and the minor axis (the longest distance perpendicular to the major axis) of each spheroid were measured. On day 9, 34 spheroids were collected from both the Matrigel and HA-PEGDT-Matrigel groups. On day 16, 25 spheroids were collected from each group. Quantitative analysis of the major axis length, minor axis length, and aspect ratio (major axis/minor axis) was performed, and the mean  $\pm$  SD was plotted. Statistical analysis was conducted using a two-tailed unpaired Student's t-test, with  $p < 0.05$  defined as statistically significant. Different levels of significance were indicated based on p-values (from \* $p < 0.05$  to \*\*\*\* $p < 0.0001$ ). The uniformity of spheroids formed in different hydrogels can be assessed by the size of the SD.

**Flow Cytometry:** The human iPSCs were incubated with Accutase (STEMCELL Technologies, Germany) at 37 °C to achieve single cell suspension. Cells were centrifuged and resuspended in 3.7% paraformaldehyde (PFA, w/v in PBS, Sigma-Aldrich, Germany) at room temperature for 10 min and permeabilized with 0.2% v/v Triton X-100 (Sigma-Aldrich, Germany) for another 10 min. MACS BSA Stock was used for diluting antibodies (isotype-APC control, anti-NANOG-APC, anti-OCT3/4-APC, Miltenyi Biotec, Germany). Cells were incubated with antibodies for 15 min at 4 °C. The fluorescence labeled cells were plotted using a MACQuant Analyzer 10 (Miltenyi Biotec, Germany) and the data was analyzed with the FlowJo software (version 10.8.1; BD Biosciences, Germany).

**RNA Extraction and Quantitative PCR:** Total RNAs from cells were extracted using TRIzol Reagent (Thermo Fisher Scientific, Germany). The reverse transcription process was performed with the Verso cDNA synthesis kit (Thermo Fisher Scientific, Germany), following the manufacturer's instructions. Quantitative PCR reactions were conducted in triplicate on a StepOnePlus real-time PCR System (Applied Biosystems, Germany). CT (threshold cycle) values higher than 35 were considered as absence of gene expression and were excluded. The CT value of 18S rRNA house-keeping gene in each sample was used to normalize the  $\Delta\text{CT}$  values of the target genes ( $\Delta\text{CT} = \text{CT}_{\text{target}} - \text{CT}_{18\text{S rRNA}}$ ). The fold change for the same gene between different time points (Time 2/Time 1) was expressed as  $2^{-\Delta\Delta\text{CT}}$  ( $\Delta\Delta\text{CT} = \Delta\text{CT}_{\text{target, Time 2}} - \Delta\text{CT}_{\text{target, Time 1}}$ ). Primers used for the detection of OCT4 (Hs00791255\_CE), NANOG (Hs00760594\_CE), FOXA2 (Hs00815707\_CE), SOX17 (Hs00683295\_CE) were purchased from Thermo Fisher Scientific, Germany.

**Cryosection, Immunostaining, and Chemical Dyes:** Samples were fixed with 3.7% w/v PFA (Sigma-Aldrich, Germany) and then embedded in frozen embedding medium (6769 006; Thermo Fisher Scientific, Germany), snap frozen and sliced to 12  $\mu\text{m}$  thickness using Microm freezing microtome HM 560 (Thermo Fisher Scientific, Germany). Cryosections were permeabilized with 0.2% v/v Triton X-100 (Sigma-Aldrich, Germany) and blocked in 5% w/v BSA, incubated with primary antibodies (listed in Table 1), which diluted in Antibody Diluent with Background Reducing Components (S302283-2; Dako GmbH, Germany) overnight at 4 °C.

**Table 1.** List of primary antibodies.

Primary antibody	Host/Isotype	Supplier	Catalog no.	Dilution
CPM	Mouse/IgG1	Thermo Fisher Scientific	MA5-26863	1:200
CCSP	Rabbit/IgG	Sigma-Aldrich	SAB2108213	1:100
FOXA2	Rabbit/IgG	CST	8186S	1:400
Active ITGB1	Mouse/IgG2b	Millipore	MAB2079Z	1:200
NMHC IIA	Rabbit/IgG	CST	3403S	1:50
NKX2.1	Rabbit/IgG	Thermo Fisher Scientific	PA5-25940	1:200
OCT4	Mouse/IgG1	Thermo Fisher Scientific	MA1-104	1:500
PIEZO1	Rabbit/IgG	Novus Biologicals	NBP1-78446	1:100
RRAS	Rabbit/IgG	CUSABIO	CSB-PA020513PA01HU	1:30
SPC	Rabbit/IgG	Thermo Fisher Scientific	PA5-71680	1:25
SPC	Mouse/IgG2a, $\kappa$	Novus Biologicals	H00006440-M01	1:50
SOX17	Mouse/IgG1	Thermo Fisher Scientific	MA5-24885	1:100
SOX2	Rabbit/IgG	Millipore	AB5603	1:200

Subsequently, secondary antibody staining was performed at room temperature for 1 h. F-actin in cells was stained using CellMask Orange Actin Tracking Stain (A57244; Thermo Fisher Scientific, Germany). Nuclei were counterstained with Hoechst 33 342 (H3570; Thermo Fisher Scientific, Germany). Unless stated otherwise, images are representative of specimens obtained from at least 8 biological replicates across 3 individual experiments. Microscopic images were captured with the TCS SP8 (Leica Microsystems, Germany) and the LSM 780 (Carl Zeiss AG, Germany) Confocal Microscope.

The raw fluorescence image datasets were imported to ImageJ software with Bio-Formats Importer plugin (National Institutes of Health, USA) for quantitative analysis.

**Statistics:** Statistical analysis was performed using two-tailed unpaired Student t-test for two groups, and one-way ANOVA with Bonferroni's multiple comparisons test for multiple group comparison (GraphPad Software, Dotmatics, USA). In all cases, p values of less than 0.05 were considered statistically significant and indicated using different thresholds (\* $p < 0.05$ , \*\* $p < 0.01$ , \*\*\* $p < 0.001$ , \*\*\*\* $p < 0.0001$ ). Quantitative data are expressed as the mean  $\pm$  standard deviation (SD) of at least three biological replicates.

## Acknowledgements

The authors express their gratitude to Professor Francesca Toma for her facilitation and support in continuing the research. Additionally, the authors acknowledge the Core Unit Pluripotent Stem Cells and Organoids (CUSCO, Berlin Institute of Health at Charité, Berlin, Germany) for generating and providing the source human iPS cells. This work was financially supported by the Helmholtz Association of German Research Centers through program-oriented funding, Helmholtz Imaging Project "AIOrganoid", China Scholarship Council (No. 202208320106) and Helmholtz Association – Munich School for Data Science (MUDS).

## Conflict of Interest

The authors declare no conflict of interest.

## Data Availability Statement

The data that support the findings of this study are available from the corresponding author upon reasonable request.

## Keywords

biomechanics, hyaluronic acid (HA), hydrogel, lung organoid, piezo1

Received: February 29, 2024

Revised: July 5, 2024

Published online:

- [1] G. B. D. C. R. D. Collaborators, *Lancet Respir. Med.* **2020**, *8*, 585.
- [2] S. J. Virolainen, A. VonHandorf, K. Viel, M. T. Weirauch, L. C. Kottyan, *Genes Immun.* **2023**, *24*, 1.
- [3] C. E. Barkauskas, M. I. Chung, B. Fioret, X. Gao, H. Katsura, B. L. Hogan, *Development.* **2017**, *144*, 986.
- [4] a) S. Youhanna, A. M. Kemas, L. Preiss, Y. Zhou, J. X. Shen, S. D. Cakal, F. S. Paqualini, S. K. Goparaju, R. Z. Shafagh, J. U. Lind, C. M. Sellgren, V. M. Lauschke, *Pharmacol. Rev.* **2022**, *74*, 141; b) B. L. LeSavage, R. A. Suhar, N. Broguiere, M. P. Lutolf, S. C. Heilshorn, *Nat. Mater.* **2022**, *21*, 143; c) H. Fan, U. Demirci, P. Chen, *J. Hematol. Oncol.* **2019**, *12*, 142; d) C. Corro, L. Novellasdemunt, V. S. W. Li, *Am. J. Physiol. Cell Physiol.* **2020**, *319*, C151.
- [5] A. J. Miller, B. R. Dye, D. Ferrer-Torres, D. R. Hill, A. W. Overeem, L. D. Shea, J. R. Spence, *Nat. Protoc.* **2019**, *14*, 518.
- [6] S. X. Huang, M. D. Green, A. T. de Carvalho, M. Mumau, Y. W. Chen, S. L. D'Souza, H. W. Snoeck, *Nat. Protoc.* **2015**, *10*, 413.
- [7] M. J. Kratochvil, A. J. Seymour, T. L. Li, S. P. Pasca, C. J. Kuo, S. C. Heilshorn, *Nat. Rev. Mater.* **2019**, *4*, 606.
- [8] A. C. Duarte, E. C. Costa, H. A. L. Filipe, S. M. Saraiva, T. Jacinto, S. P. Miguel, M. P. Ribeiro, P. Coutinho, *Biomater. Adv.* **2023**, *151*, 213428.
- [9] Z. Dai, Y. Peng, H. A. Mansy, R. H. Sandler, T. J. Royston, *Med. Eng. Phys.* **2015**, *37*, 752.
- [10] a) A. Suo, W. Xu, Y. Wang, T. Sun, L. Ji, J. Qian, *Carbohydr. Polym.* **2019**, *217*, 336; b) A. Yasin, Y. Ren, J. Li, Y. Sheng, C. Cao, K. Zhang, *Front. Bioeng. Biotechnol.* **2022**, *10*, 910290.
- [11] a) Z. Gan, X. Qin, H. Liu, J. Liu, J. Qin, *Bioact. Mater.* **2023**, *28*, 386; b) K. Hillion, M. M. Mahe, *Nat. Methods.* **2022**, *19*, 1347; c) A. R. Cameron, J. E. Frith, G. A. Gomez, A. S. Yap, J. J. Cooper-White, *Biomaterials.* **2014**, *35*, 1857; d) Y. Zhang, Z. Wang, Q. Sun, Q. Li, S. Li, X. Li, *Materials (Basel).* **2023**, *16*, 5161; e) N. Broguiere, L. Isenmann, C. Hirt, T. Ringel, S. Placzek, E. Cavalli, F. Ringnalda, L. Villiger, R. Zulliger,

- R. Lehmann, G. Rogler, M. H. Heim, J. Schuler, M. Zenobi-Wong, G. Schwank, *Adv. Mater.* **2018**, *30*, 1801621.
- [12] D. T. Butcher, T. Alliston, V. M. Weaver, *Nat. Rev. Cancer.* **2009**, *9*, 108.
- [13] H. Fagman, E. Amendola, L. Parrillo, P. Zoppoli, P. Marotta, M. Scarfo, P. De Luca, D. P. de Carvalho, M. Ceccarelli, M. De Felice, R. Di Lauro, *Dev. Biol.* **2011**, *359*, 163.
- [14] C. Gontan, A. de Munck, M. Vermeij, F. Grosveld, D. Tibboel, R. Rottier, *Dev. Biol.* **2008**, *317*, 296.
- [15] S. Gotoh, I. Ito, T. Nagasaki, Y. Yamamoto, S. Konishi, Y. Korogi, H. Matsumoto, S. Muro, T. Hirai, M. Funato, S. Mae, T. Toyoda, A. Sato-Otsubo, S. Ogawa, K. Osafune, M. Mishima, *Stem Cell Rep.* **2014**, *3*, 394.
- [16] P. He, K. Lim, D. Sun, J. P. Pett, Q. Jeng, K. Polanski, Z. Dong, L. Bolt, L. Richardson, L. Mamanova, M. Dabrowska, A. Wilbrey-Clark, E. Madisson, Z. K. Tuong, E. Dann, C. Suo, I. Goh, M. Yoshida, M. Z. Nikolic, S. M. Janes, X. He, R. A. Barker, S. A. Teichmann, J. C. Marioni, K. B. Meyer, E. L. Rawlins, *Cell.* **2022**, *185*, 4841.
- [17] a) M. Herriges, E. E. Morrisey, *Development.* **2014**, *141*, 502; b) J. C. Schittny, *Cell Tissue Res.* **2017**, *367*, 427; c) E. E. Morrisey, B. L. Hogan, *Dev. Cell.* **2010**, *18*, 8.
- [18] B. R. Dye, J. T. Decker, R. F. C. Hein, A. J. Miller, S. Huang, J. R. Spence, L. D. Shea, *Tissue Eng. Part A.* **2022**, *28*, 893.
- [19] a) Z. M. Shao, P. De Coppi, F. Michielin, *Front Chem Eng.* **2023**, *5*, 1255783; b) C. M. Waters, E. Roan, D. Navajas, *Compr. Physiol.* **2012**, *2*, 1.
- [20] J. Bhattacharya, R. F. Hough, *Am. J. Respir. Cell Mol. Biol.* **2019**, *60*, 609.
- [21] a) J. Li, Z. Wang, Q. Chu, K. Jiang, J. Li, N. Tang, *Dev. Cell.* **2018**, *44*, 297; b) B. L. M. Hogan, *Dev. Cell.* **2018**, *44*, 273; c) Z. Tang, Y. Hu, Z. Wang, K. Jiang, C. Zhan, W. F. Marshall, N. Tang, *Dev. Cell.* **2018**, *44*, 313.
- [22] a) B. J. McHugh, R. Buttery, Y. Lad, S. Banks, C. Haslett, T. Sethi, *J. Cell Sci.* **2010**, *123*, 51; b) M. Yao, A. Tijore, D. Cheng, J. V. Li, A. Hariharan, B. Martinac, G. Tran Van Nhieu, C. D. Cox, M. Sheetz, *Sci. Adv.* **2022**, *8*, eabo1461; c) A. Allen, R. Maddala, C. Eldawy, P. V. Rao, *Int. J. Mol. Sci.* **2022**, *23*, 4710; d) M. A. Conti, R. S. Adelstein, *J. Cell Sci.* **2008**, *121*, 11.
- [23] K. L. Ellefsen, J. R. Holt, A. C. Chang, J. L. Nourse, J. Arulmoli, A. H. Mekhdjian, H. Abuwarda, F. Tombola, L. A. Flanagan, A. R. Dunn, I. Parker, M. M. Pathak, *Commun. Biol.* **2019**, *2*, 298.
- [24] a) C. J. Aros, C. J. Pantoja, B. N. Gomperts, *Commun. Biol.* **2021**, *4*, 601; b) K. Lim, A. P. A. Donovan, W. Tang, D. Sun, P. He, J. P. Pett, S. A. Teichmann, J. C. Marioni, K. B. Meyer, A. H. Brand, E. L. Rawlins, *Cell Stem Cell.* **2023**, *30*, 20; c) N. Ahmadvand, A. Lingampally, F. Khosravi, A. I. Vazquez-Armendariz, S. Rivetti, M. R. Jones, J. Wilhelm, S. Herold, G. Barreto, J. Koepke, C. Samakovlis, G. Carraro, J. S. Zhang, D. Al Alam, S. Bellusci, *Cell. Mol. Life Sci.* **2022**, *79*, 302; d) J. R. Rock, X. Gao, Y. Xue, S. H. Randell, Y. Y. Kong, B. L. Hogan, *Cell Stem Cell.* **2011**, *8*, 639.
- [25] a) C. J. Rendon, E. Flood, J. M. Thompson, M. Chirivi, S. W. Watts, G. A. Contreras, *Front. Endocrinol.* **2022**, *13*, 995499; b) E. T. Hall, E. Hoising, E. Sinkovics, E. M. Verheyen, *Mol. Biol. Cell.* **2019**, *30*, 411.
- [26] K. Mieczkowski, M. Popeda, D. Lesniak, R. Sadej, K. Kitowska, *J. Mammary Gland Biol. Neoplasia.* **2023**, *28*, 9.
- [27] H. Kiyokawa, M. Morimoto, *Dev. Growth Differ.* **2020**, *62*, 67.
- [28] G. L. Hunter, L. He, N. Perrimon, G. Charras, E. Giniger, B. Baum, *BMC Biol.* **2019**, *17*, 12.
- [29] a) C. Grannemann, A. Pabst, A. Honert, J. Schieren, C. Martin, S. Hank, S. Boll, K. Blasius, S. Dusterhoft, H. Jahr, R. Merkel, R. Leube, A. Babendreyer, A. Ludwig, *Biomater. Adv.* **2023**, *152*, 213516; b) V. Caolo, M. Debant, N. Endesh, T. S. Futers, L. Lichtenstein, F. Bartoli, G. Parsonage, E. A. Jones, D. J. Beech, *Elife.* **2020**, *9*, e50684; c) D. Choi, E. Park, R. P. Yu, M. N. Cooper, I. T. Cho, J. Choi, J. Yu, L. Zhao, J. I. Yum, J. S. Yu, B. Nakashima, S. Lee, Y. J. Seong, W. Jiao, C. J. Koh, P. Baluk, D. M. McDonald, S. Saraswathy, J. Y. Lee, N. L. Jeon, Z. Zhang, A. S. Huang, B. Zhou, A. K. Wong, Y. K. Hong, *Circ. Res.* **2022**, *131*, e2.
- [30] C. Loebel, A. I. Weiner, M. K. Eiken, J. B. Katzen, M. P. Morley, V. Bala, F. L. Cardenas-Diaz, M. D. Davidson, K. Shiraishi, M. C. Basil, L. T. Ferguson, J. R. Spence, M. Ochs, M. F. Beers, E. E. Morrisey, A. E. Vaughan, J. A. Burdick, *Adv. Mater.* **2022**, *34*, 2202992.
- [31] S. K. Seidlits, Z. Z. Khaing, R. R. Petersen, J. D. Nickels, J. E. Vanscoy, J. B. Shear, C. E. Schmidt, *Biomaterials.* **2010**, *31*, 3930.
- [32] X. Xu, Y. Nie, W. Wang, I. Ullah, W. T. Tung, N. Ma, A. Lendlein, *Clin. Hemorheol. Microcirc.* **2021**, *79*, 217.
- [33] R. F. C. Hein, A. S. Conchola, A. S. Fine, Z. Xiao, T. Frum, L. K. Brastrom, M. A. Akinwale, C. J. Childs, Y. H. Tsai, E. M. Holloway, S. Huang, J. Mahoney, I. Heemskerck, J. R. Spence, *Development.* **2022**, *149*, dev200693.